

Mechanism and Kinetics of Aluminum Nitride Powder Degradation in Moist Air

Jinwang Li,^{*,†} Masaru Nakamura, Takashi Shirai, Koji Matsumaru, Chanel Ishizaki,[‡] and Kozo Ishizaki*

School of Mechanical Engineering, Nagaoka University of Technology, Nagaoka, Niigata 940-2188, Japan

Aluminum nitride (AlN) powders manufactured via three major commercial processes, namely, chemical vapor deposition from triethyl aluminum, carbothermal reduction and nitridation of alumina, and direct nitridation of aluminum, were exposed to moist air at room temperature to investigate the degradation mechanism and kinetics. In the degradation, the powders were initially hydrolyzed to amorphous aluminum oxyhydroxide, which subsequently transformed into mixtures of crystallized aluminum trihydroxide (Al(OH)₃) polymorphs, i.e., bayerite, nordstrandite, and gibbsite, forming agglomerates around the unreacted AlN. The data were fitted by using the unreacted-core model. Three stages were found in the degradation: the stage of an induction period at the beginning, followed by a stage of fast hydrolysis with the chemical reaction being rate controlling, and finally, with gradual closing of pores in the structure of Al(OH)₃ around AlN, changing to a stage of slow hydrolysis that was controlled by mass diffusion through Al(OH)₃. The existence of an induction period was attributed to slow hydrolysis of the surface oxide/oxyhydroxide layer. The powder produced by the carbothermal process showed the longest induction period, which was attributed to its surface structure being different from other powders.

I. Introduction

ALUMINUM NITRIDE (AlN) is an important material for substrates in electronic devices because of its high intrinsic thermal conductivity ($320 \text{ W} \cdot (\text{m} \cdot \text{K})^{-1}$),¹ its thermal expansion coefficient being close to that of silicon, and its excellent electric and dielectric properties.^{2,3} The thermal conductivity of sintered AlN is greatly reduced by oxygen contamination in AlN grains, because oxygen occupation in AlN lattices generates vacancies that work as phonon-scattering sites.^{1,4–7} Low-oxygen AlN powders are preferred for achieving high thermal conductivity. Efforts have been made to prepare high-purity AlN powders with a low oxygen content, and such powders have been commercially available. Unfortunately, because AlN is unstable in a water-containing environment, oxygen contamination arises not only from the powder manufacturing process but also from contact with water molecules in powder processing after manufacturing.

Many researchers have investigated the degradation of AlN powders in water and water-based solutions. These studies have focused on the reaction mechanism and kinetics,^{8,9} the influence of pH,¹⁰ the effect of different solutes,^{11,12} the formation of a protective oxide^{13,14} or organic^{15,16} layer, and the influence of

oxygen content in AlN powder.¹⁷ In contrast, degradation of AlN powders in ambient atmospheres at room temperature has been much less studied. Abid *et al.*¹⁸ reported that AlN did not readily react with atmospheric moisture at room temperature. On the other hand, Kameshima *et al.*¹⁹ found, using X-ray photoelectron spectrometry (XPS), that the surface of AlN powders reacted slowly with atmospheric moisture during several years of storage in a capped container.

A thorough understanding of the degradation mechanism and kinetics for AlN powders under atmospheric conditions is fundamental for appropriate powder processing. Unfortunately, research reports for this purpose are hitherto unavailable, in contrast to numerous publications on AlN powder preparation, oxidation at elevated temperatures, sintering, etc. Keeping this in mind, we studied the degradation mechanism and kinetics of AlN powders in moist air at room temperature. The purpose of our research was twofold. First, we wished to provide the degradation chemistry of AlN powder under atmospheric conditions. Second, we wished to clarify the influence of the powder surface structure, which was determined to depend on the manufacturing process,^{20,21} on the degradation. Thus, we used powders produced via three major commercial processes, whose effect on the surface structure was studied before.^{20,21} The initial stage of the degradation was well correlated to the surface structure.

The analyses of the phase composition of the degradation products using X-ray diffraction (XRD) and diffuse reflectance infrared Fourier transform spectroscopy (DRIFT) techniques have been discussed in a previous report.²² This paper places emphasis on the analysis of the degradation mechanism and kinetics.

II. Experimental Procedure

The five AlN powders studied are listed in Table I. These powders were produced through three major commercial approaches: chemical vapor deposition (CVD) from triethyl aluminum (powder A of grade MAN-2, Mitsui Chemicals Inc., Tokyo, Japan), carbothermal reduction and nitridation of alumina (powders B1 of grade H and B2 of grade F, Tokuyama Corp., Tokyo, Japan), and direct nitridation of aluminum metal (powders C1 of grade B and C2 of grade C, H.C. Starck GmbH, Goslar, Germany). After the powders were obtained from the manufacturers, they were stored in a high-purity nitrogen atmosphere. During the degradation, the powder samples, each spread with a maximum thickness of less than 2 mm on a glass dish, were held above distilled water in a glass vessel at atmospheric pressure. The glass vessel was loosely capped to allow the release of gaseous ammonia product. The laboratory temperature and relative humidity were controlled at 20°C and 30%, respectively. The relative humidity around the samples was monitored to be 80% during the degradation. Many samples were prepared for each powder, and each sample was used to measure for a point in the mass change–time curve (Fig. 1 shown in the next section). After a certain period of degradation one sample of each powder was taken out of the glass vessel and dried at 100°C for 2 h in air. This drying condition proved to be sufficient as on further heating at 160°C, mass change was not

N. Jacobson—contributing editor

Manuscript No. 20452. Received April 22, 2005; approved August 9, 2005.

This work was financially supported by the Ministry of Education, Culture, Sports, Science and Technology through the 21st Century Center of Excellence (COE) Program.

*Member, American Ceramic Society.

[†]Author to whom correspondence should be addressed. e-mail: jwli@msl.titech.ac.jp. Present address: Materials and Structures Laboratory, Tokyo Institute of Technology, 4259-R3-20 Nagatsuta, Midori-ku, Yokohama 226-8503, Japan.

[‡]Permanent address: Nano TEM Co. Ltd., Shimogajo 1-485, Nagaoka, Niigata 940-0012, Japan.

Table I. Characteristics of the Aluminum Nitride Powders Investigated in This Study

	Chemical vapor deposition		Carbothermal reduction and nitridation of Al ₂ O ₃		Direct nitridation of aluminum	
	A		B1	B2	C1	C2
Specific surface area (m ² /g)	2.0		2.63	3.31	2.8	4.0
Mean particle size (μm)	3.0		1.55	1.3	3.25	2.41
O (wt%)	0.37		0.83	0.89	1.14	1.6
C (wt%)	0.04		0.022	0.039	0.05	0.04
Si (ppm, wt)	23		38	<9	—	—
Fe (ppm, wt)	<10		10	<10	<20	20
Ca (ppm, wt)	—		220	6	—	—

observed. XRD analysis indicated that the drying process did not change the phase composition.

Sample masses were measured before degradation and after drying. The mass change, Δm , in the degradation was expressed as

$$\Delta m = \frac{m_t - m_0}{m_0} \times 100\% \quad (1)$$

where m_t is the mass of the dried sample after degradation for period t , and m_0 the initial mass. Thermogravimetric/differential thermal analysis (TG/DTA) for the degraded powders was performed in a nitrogen atmosphere up to 500°C at a heating rate of 10 K/min on a simultaneous TG-DTG-DTA instrument (model TG/DTA6200, Seiko Instruments Inc., Chiba, Japan). Scanning electron microscopy (SEM) for microstructural observation was conducted on a Keyence VE 7800 microscope (Keyence Corp., Osaka, Japan). Brunauer-Emmett-Teller (BET) surface areas were measured on a Shimadzu Micromeritics Flow Sorb 2300 analyzer (Shimadzu Corp., Kyoto, Japan).

III. Results and Discussion

(1) Mass Change and Degradation Reactions

The mass changes of AlN powders during degradation are shown in Fig. 1. The masses of all powders increased with degradation time. The mass increase was because of hydrolysis of AlN to form aluminum hydroxides,²² as described below. In the beginning, each powder underwent an induction period when the degradation was slow. With increasing time, the degradation rate increased at first, and then gradually decreased. The mass change-time curves were S shaped. The powders from the carbothermal process showed the longest induction period.

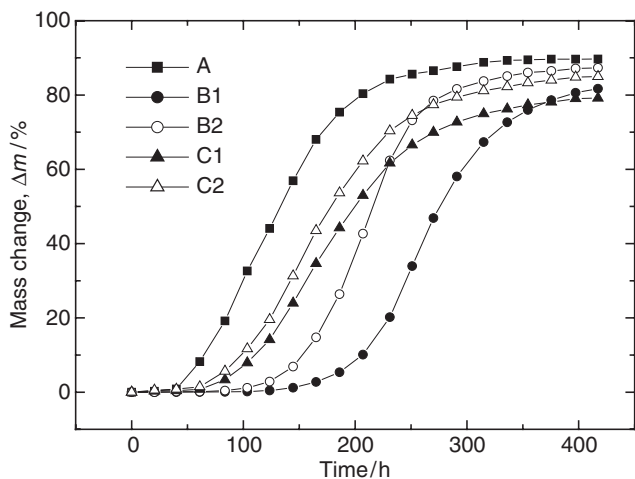


Fig. 1. Mass change in the degradation of the aluminum nitride powders in moist air (80% humidity) at 20°C.

For each AlN powder, at the beginning of degradation ($\Delta m < \sim 2\%$), no crystallized products were detected by XRD, and DRIFT analysis showed the formation of amorphous aluminum oxyhydroxide (AlOOH).²² XRD and DRIFT analyses revealed the formation of a mixture of polymorphs of aluminum trihydroxide (Al(OH)₃), namely bayerite, nordstrandite, and gibbsite, at different conversions when $\Delta m > \sim 2\%$,²² indicating AlOOH \rightarrow Al(OH)₃ conversion following AlOOH formation. In the hydrolysis of AlN powders in water at room temperature, Bowen *et al.*⁹ also observed the formation of amorphous AlOOH up to 8 h (>20% conversion) of hydrolysis, which later transformed into crystalline bayerite. Amorphous AlOOH acted as an intermediate product in the hydrolysis. AlOOH \rightarrow Al(OH)₃ conversion has also been observed in the corrosion of aluminum by liquid or gaseous water at room temperature.^{23,24}

Accordingly, the overall hydrolysis reaction was



(Ammonia gas was detected during the degradation.) Similar to what was proposed by Bowen *et al.*⁹ in their study on the hydrolysis of AlN powders in water at room temperature, the reaction could proceed in two steps as follows:



(2) TG/DTA

TG/DTA analysis was performed in order to detect whether appreciable amounts of amorphous AlOOH were present in the products after the formation of crystalline Al(OH)₃ phases ($\Delta m > \sim 2\%$). The TG/DTA analysis results up to 500°C showed similar results for different powders at various Δm values. A typical result is shown in Fig. 2. A strong endothermic

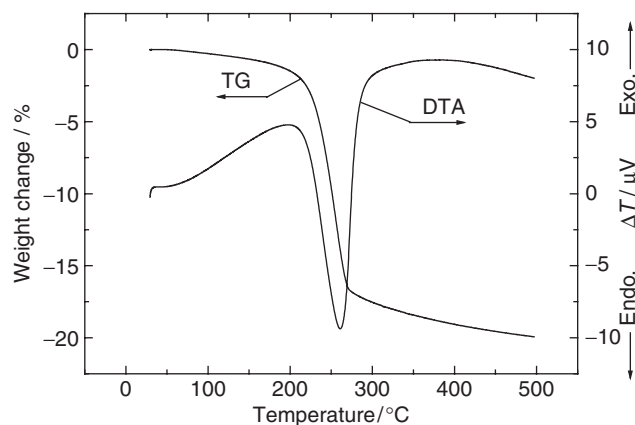


Fig. 2. Typical thermogravimetric/differential thermal analysis result (from degraded powder B2 at $\Delta m = 43.4\%$) of degraded powders.

peak from 200° to 300°C, centered at 261°C, accompanied by a sharp weight loss, was because of the decomposition of Al(OH)₃ phases to transition alumina.²⁵ The weight losses observed up to 500°C were consistent with the values calculated by assuming a stoichiometry of Al(OH)₃ for the hydrolysis products, indicating no appreciable AlOOH in the products. (If appreciable amounts of AlOOH had existed in the products, the observed weight losses would have been much less than the calculated ones.) Small differences were found, i.e., the calculated values were ~0.2% (for low Δm achieved in hydrolysis) to 3% (for high Δm) larger than the measured ones, which may have been caused by the presence of small amounts of AlOOH and/or incomplete dehydration, as indicated by the TG curves that show progressive weight loss to continue beyond 500°C. In fact, progressive dehydroxylation could continue up to the corundum-formation temperature (~1100°C).²⁵ The value of Δm of powder A (89.7%) after 417 h of degradation was in good agreement with the calculated value (90.3% for the complete conversion of pure AlN to Al(OH)₃). The small difference could be attributed to impurities, e.g., 0.37 wt% oxygen, in the raw powder. Mass changes of the other four powders after the same period of degradation (B1 81.7%, B2 87.3%, C1 79.2%, and C2 85.0%) were less than the calculated values, which was because of incomplete hydrolysis as evidenced by the presence of AlN reflections in their XRD patterns (not shown). In sum, no appreciable AlOOH was detected, and Al(OH)₃ accounted for the major composition in the hydrolysis products after formation of crystallized trihydroxide phases. This could have been because the amorphous AlOOH was only an intermediate product as observed in the beginning of the degradation, and existed only as a thin layer on the surface of the unreacted AlN.

Therefore, the fractional conversion after formation of crystalline Al(OH)₃ phases, used in the section for kinetics analysis below, was calculated as the measured mass change divided by the calculated mass change for complete conversion of AlN to Al(OH)₃.

(3) Microstructural Evolution

Figures 3(a)–(i) show the microstructural evolution during degradation for some representative powders. Although the microstructures of raw powders differed from one manufacturing method to another, the microstructure evolution shared some common features. Evidently, the surfaces of the powders were hydrolyzed first, resulting in agglomeration of the parent particles. It was reported that formation of hard agglomerates in α -alumina powder was because of the hydrolysis of the surface to produce Al(OH)₃, which formed a hydrogen bonding, and subsequently produced a crystalline structure similar to polymorphs of Al(OH)₃, between adjacent particles.²⁶ This mechanism could be envisaged in agglomerate formation in our study. Particles of Al(OH)₃ polymorphs, nucleating and growing around the parent particles and their agglomerates, began to appear at a mass change of a few percent and subsequently formed agglomerates as well. As a result, the agglomerates formed by the reaction products became larger as the hydrolysis proceeded, enveloping the unreacted AlN inside.

A difference could be observed in the microstructural development between powders from the carbothermal process and the other powders. The former ones developed agglomerates that were more uniform in size. This might have been caused by differences in the microstructure of the parent AlN powders. As shown in Fig. 3, raw powder A was severely agglomerated, and the powders from the direct nitridation process had very broad size distributions. In contrast, the powders from the carbothermal process were the smallest and the most uniform in size, which may result in formation of agglomerates of a narrower size distribution.

(4) Influence of Surface Structure on Induction Period

The existence of an induction period in the hydrolysis may be related to the surface structure of AlN powders. Using the tech-

niques of temperature-programmed desorption mass spectroscopy (TPDMS) and auger electron spectroscopy (AES), and by comparing the desorption behaviors and AES spectra of AlN powders with those of oxynitride, α -alumina, θ -alumina, γ -alumina, and boehmite, Ishizaki *et al.* found that the surface of AlN powders produced by the carbothermal process was composed of a θ -alumina-like layer containing oxynitride, and those from CVD and direct nitridation were composed of an γ -alumina-like or boehmite-like layer and an oxygen-diffused layer.^{20,21} On the other hand, in the investigation of the surface change during storage over years using XPS analysis, Kameshima *et al.*¹⁹ concluded that the surfaces of AlN powders from the carbothermal or direct nitridation processes were composed of an γ -alumina-like layer. However, they did not use θ -alumina and boehmite for reference and ignored the difference in chemical shifts that was observed in their XPS results between powders from carbothermal and direct nitridation processes. (CVD powder was not used in their study.) Nevertheless, it is clear that an oxide/hydroxide layer covers AlN powder surfaces. The continuous and amorphous oxide/oxyhydroxide layer could protect the AlN against corrosion. The induction period could be because of a slow process to hydrolyze this surface layer, during which surface oxide might be first hydrolyzed to amorphous AlOOH, and slow diffusion of water through the layer to react with AlN might also occur to form amorphous AlOOH, followed by AlOOH \rightarrow Al(OH)₃ conversion. Kameshima *et al.*¹⁹ also proposed a final conversion of the surface aluminum oxide to trihydroxide in AlN powder degradation during storage in a capped container.

A thicker and more stable oxide surface layer was expected to protect AlN particles better. Kameshima *et al.*¹⁹ reported that the powders from the carbothermal process had better resistance to weathering, and attributed this to a thicker surface oxide layer (after measurement of this layer using XPS) than the ones produced by direct nitridation. Some authors reported that an oxide surface layer on AlN powders formed by heat treatment at >800°C improved hydrolysis resistance in water.^{13,14} TPDMS analysis indicated that, unlike powders produced by CVD and direct nitridation processes, the powder produced by the carbothermal process showed no desorption of NH₃,²⁰ demonstrating its better resistance to moisture attack because of the higher stability of its surface structure. Our observation that the powders from the carbothermal process (powders B1 and B2) showed the longest induction periods (Fig. 1) could thus be attributed to their θ -alumina-like and/or thicker surface layer being different from the γ -alumina-like or boehmite-like surface layers of the other powders. The transformation sequence of the aluminum oxide/hydroxide with increasing temperature is boehmite \rightarrow γ -alumina \rightarrow δ -alumina \rightarrow θ -alumina \rightarrow α -alumina,²⁵ where α -alumina is the most stable phase. This may suggest that the θ -alumina structure is more stable than the γ -alumina or boehmite one in the degradation.

(5) Kinetics Analysis

The degradation kinetics after the induction period were analyzed by using the unreacted-core model.²⁷ In this model, the reaction starts at the outer surface of the particle and moves inward, resulting in an increasing layer of the solid product covering the shrinking unreacted core. For an irreversible reaction, there are three steps contributing directly to the resistance to reaction: (a) mass transfer of the fluid reactant through the fluid film surrounding the particle to the surface of the solid, (b) penetration and diffusion of the fluid reactant through the product layer to the surface of the unreacted core, and (c) chemical reaction of the fluid reactant with the unreacted core at the core surface. The slowest step is rate controlling. Kinetic equations for rate controlling by each of these steps, developed without considering the volume difference between the reacted parent solid and the product solid layer, have been introduced by Levenspiel.²⁷ These equations have been able to describe a variety of gas–solid systems.²⁷ Nevertheless, ignoring the volume

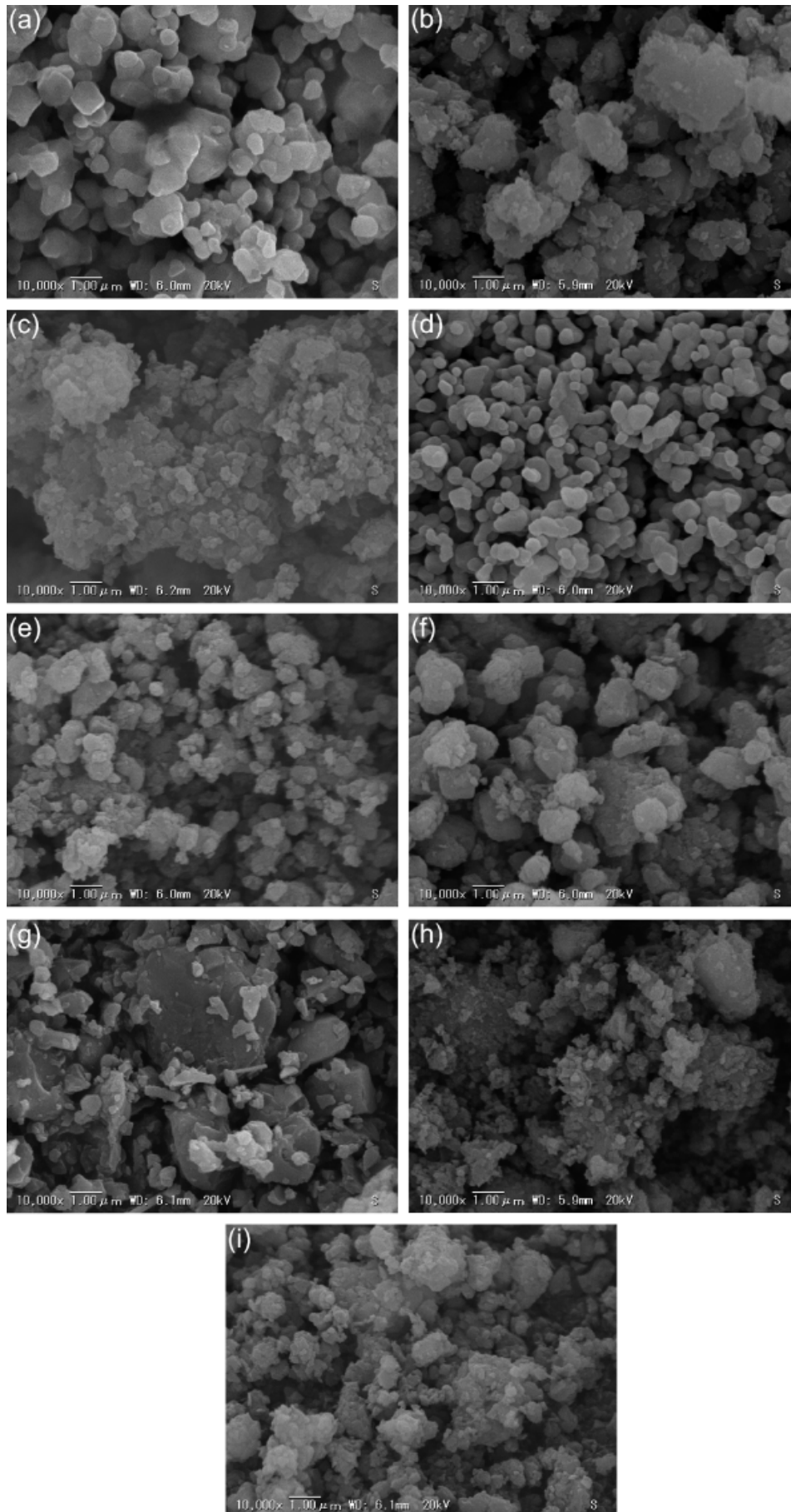


Fig. 3. Scanning electron microscopy observation of raw ($\Delta m = 0\%$) and hydrolyzed powders: powder A at $\Delta m = 0\%$ (a), 8.0% (b), and 89.7% (c); powder B2 at $\Delta m = 0\%$ (d), 43.4% (e), and 87.3% (f); powder C1 at $\Delta m = 0\%$ (g), 33.3% (h), and 79.2% (i).

difference could result in inadequate fitting or wrong determination of the reaction mechanism in case of high conversion accompanied by a large volume change. After considering the volume change, Carter obtained an equation for rate controlling by step (b),^{28,29} and we developed (see Appendix A) an equation for rate controlling by step (a). Volume change does not affect the equation for rate controlling by step (c). In our analysis, a time parameter, t_0 , was introduced into these equations to correct for the induction period, i.e., time t in the original equations was expressed as $(t-t_0)$ (see Appendix A for explanation), as shown below.

(a) Mass transfer through fluid film controls:

$$X = \frac{t - t_0}{\tau_M} \quad (\text{without considering volume difference}) \quad (5)$$

$$[1 + (Z - 1)X]^{1/3} - 1 = (Z - 1)k_M(t - t_0) \quad (\text{considering volume difference}) \quad (6)$$

(b) Diffusion through product layer controls:

$$1 - 3(1 - X)^{2/3} + 2(1 - X) = \frac{t - t_0}{\tau_D} \quad (\text{without considering volume difference}) \quad (7)$$

$$[1 + (Z - 1)X]^{2/3} + (Z - 1)(1 - X)^{2/3} = Z - (Z - 1)k_D(t - t_0) \quad (\text{considering volume difference}) \quad (8)$$

(c) Surface chemical reaction controls:

$$1 - (1 - X)^{1/3} = \frac{t - t_0}{\tau_R} \quad (9)$$

where X is the fractional conversion, τ 's are the times for the complete reaction of a particle for each step when volume difference is ignored, k 's are rate constants, and Z is the volume of the reaction product formed per unit volume of the solid reactant. It should be noted that the familiar Jander model^{30,31} for rate controlling by diffusion through the product layer is not used here because it is appropriate only at low conversions (i.e., with thin product layers) because of a simplification in its development: the diffusion layer was simplified to a plane one.

In our study, X was calculated as the measured mass change divided by the calculated mass change for complete conversion of AlN into Al(OH)₃. The value of Z fell in the range 2.45–2.65 according to the molar volumes of AlN and the three polymorphs of Al(OH)₃. Data fitting by linear regression to Eqs. (5)–(9) indicated that Eq. (9) described our experimental data the best. The results of data fitting to Eq. (9) are shown in Table II and Fig. 4. The correlation coefficients obtained were very close to 1, indicating that the data were well fitted. The τ_R was predicted to be proportional to the particle size before the reaction.²⁷ The values of τ_R obtained were plotted against the particle sizes of powders (Fig. 5), suggesting that this prediction was followed. The deviation could have arisen from the simplification in the prediction that the particles are spherical and of

Table II. Results of Data Fitting by Linear Regression to Eq. (9)

Powder	Applicable time range (h)	τ_R (h)	t_0 (h)	Correlation coefficient
A	83–231	273	66	0.9988
B1	231–315	289	208	0.9996
B2	186–270	208	163	0.9977
C1	123–251	407	103	0.9994
C2	123–251	341	98	0.9994

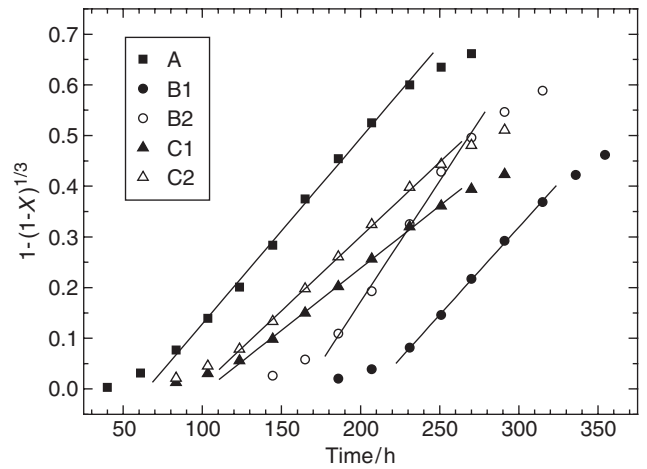


Fig. 4. Data fitting by linear regression to Eq. (9). The points show the observed data, and the straight lines were obtained from the regression.

the same size, and from the error in the measurement of particle size. For instance, powder A was severely agglomerated (Fig. 3), leading to a measured particle size (by the sedimentation method) considerably larger than the effective size in the reaction, thus resulting in a large deviation from the prediction.

Therefore, the hydrolysis reaction was controlled by a surface chemical reaction at a certain stage for each powder. The hydrolysis of AlN powders in water at room temperature has been reported to follow the same controlling mechanism up to a conversion of 80%.⁹ After this stage that was rate controlled by a chemical reaction, the reaction slowed down to a rate lower than that predicted by the model (Fig. 4). The reason for this could be as follows: the product around the unreacted AlN was porous at low conversion, as suggested by the SEM observation (Figs. 3(e) and (h)) that indicates the hydrolysis products did not become compacted densely around the AlN, leaving channels for water vapor to gain fast access to the AlN surface with little resistance. With the increase of conversion, the Al(OH)₃ particles around AlN became more and more agglomerated, and thus the pores were gradually closed. This pore-closing process with agglomeration could be analogous to the densification process in sintering, and was evidenced by denser agglomerates at high conversion with smoother surfaces (Figs. 3(c), (f), and (i)) compared with the ones at lower conversion. Specific surface areas of some hydrolyzed samples were measured to obtain more evidence. As shown in Fig. 6, the decrease of the specific surface area at high conversion supported the existence of this pore-closing process. With gradual pore-closing, the rate-controlling step changed progressively from a chemical reaction to the

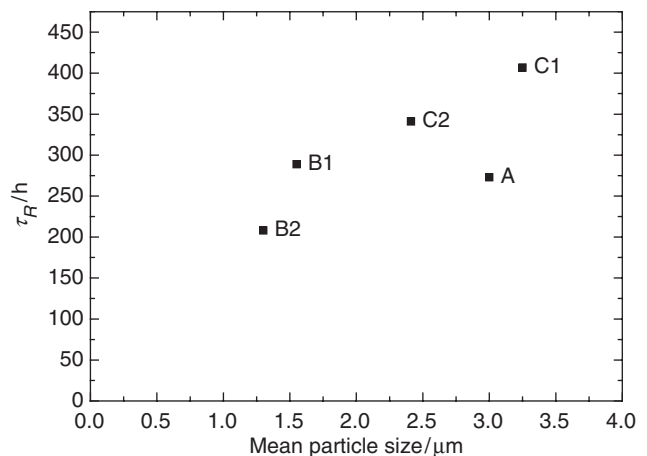


Fig. 5. Relation between τ_R and the mean particle size of aluminum nitride powders.

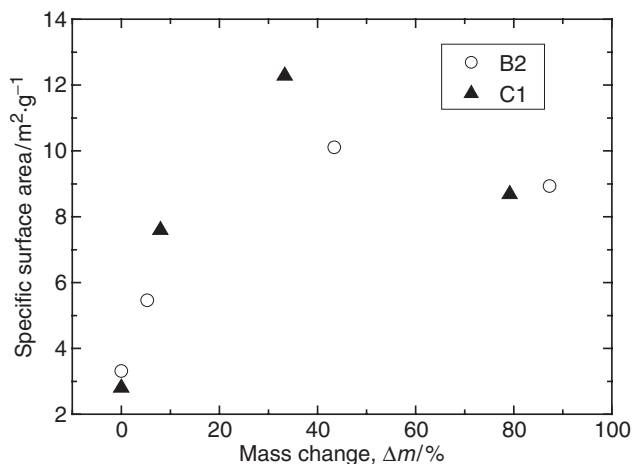


Fig. 6. Specific surface areas of samples B2 and C1 against mass changes in degradation.

diffusion of water through the $\text{Al}(\text{OH})_3$ layer. The dense $\text{Al}(\text{OH})_3$ layer thus formed around the AlN protected the unreacted AlN against fast degradation. This situation was like the protection of aluminum metal by forming a continuous aluminum hydroxide layer on the surface.²⁵ The outer part of the product layer, produced initially, had a longer pore-closing time, and thus was expected to have a denser structure than the inner part. Equations (7) and (8) did not apply to rate controlling by mass transfer through this type of structure.

In summary, three stages were found during the degradation process, starting with a stage of the induction period, followed by a stage with the chemical reaction being rate controlling, and ending with a stage that was controlled by mass transfer through the $\text{Al}(\text{OH})_3$ around the unreacted AlN .

IV. Conclusions

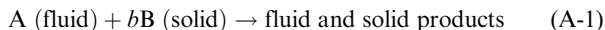
Degradation of AlN powders in moist air at room temperature undergoes three stages. The first is an induction period, during which the surface aluminum oxide/oxyhydroxide layer is slowly hydrolyzed. The length of this period is affected by the surface layer composition, which is in turn affected by the manufacturing methods. The powder produced by the carbothermal process showed the longest induction period because its surface oxide layer was thicker and/or might have been more stable. The second stage is one of fast hydrolysis controlled by a chemical reaction on the unreacted AlN surface. Gradual closing of pores in the structure of $\text{Al}(\text{OH})_3$ around AlN leads to the final stage, at which the hydrolysis rate is lower and controlled by mass transfer through the $\text{Al}(\text{OH})_3$ around the unreacted AlN .

With respect to the change of structure, we conclude that amorphous AlOOH is produced initially in the hydrolysis, and is further hydrolyzed to form mixtures of crystallized bayerite, nordstrandite, and gibbsite, agglomerating around the unreacted AlN .

Appendix A

(A.1) Development of Eq. (6)

For the reaction



where b is the stoichiometric coefficient of reactant B, the following equation has been developed in the literature for rate controlling by mass transfer through a fluid film²⁷:

$$-\frac{1}{S_{\text{ex}}} \frac{dN_B}{dt} = -\frac{\rho_B r_c^2}{R_{\text{ex}}^2} \frac{dr_c}{dt} = bk_f C_{\text{Af}} \quad (\text{A-2})$$

where S_{ex} is the area of the outer surface of the product layer around the unreacted core, N_B are the moles of B, t is the reaction time, ρ_B is the density of B, r_c is the radius of the unreacted core, R_{ex} is the radius of the outer surface of the product layer, k_f is the diffusion constant of A through the fluid film, and C_{Af} is the concentration of A around the fluid film. When the volume difference between the reacted parent solid and the product solid is ignored, $R_{\text{ex}} = R$ (starting particle radius of B), as was considered in developing Eq. (5).²⁷ Here, the volume difference is considered, and the volume decrease of B multiplied by Z is the volume increase of the product solid layer, or

$$\frac{4}{3}\pi(R^3 - r_c^3)Z = \frac{4}{3}\pi(R_{\text{ex}}^3 - r_c^3) \quad (\text{A-3})$$

On combining Eqs. (A-2) and (A-3) to eliminate R_{ex} , separating variables, and integrating, we have

$$-\rho_B \int_R^{r_c} \frac{r_c^2 dr_c}{[ZR^3 - (Z-1)r_c^3]^{2/3}} = bk_f C_{\text{Af}} \int_0^t dt$$

or

$$\frac{\rho_B R}{(Z-1)} \left\{ \left[Z - (Z-1) \left(\frac{r_c}{R} \right)^3 \right]^{1/3} - 1 \right\} = bk_f C_{\text{Af}} t \quad (\text{A-4})$$

Noting

$$1 - X = \frac{\text{volume of unreacted core}}{\text{volume of B before reaction}} = \frac{(4/3)\pi r_c^3}{(4/3)\pi R^3} = \left(\frac{r_c}{R} \right)^3$$

and letting

$$k_M = \frac{bk_f C_{\text{Af}}}{\rho_B R}$$

From Eq. (A-4) we obtain

$$[1 + (Z-1)X]^{1/3} - 1 = (Z-1)k_M t \quad (\text{A-5})$$

After rewriting t as $(t-t_0)$ to correct for the induction period, Eq. (6) is obtained.

(A.2) Correction for the Induction Period

Figure A1 shows that the experimental data follow a kinetic model in the time range t_1 to t_2 . The time parameter, t_0 , used in this study for correction for the induction period, was different

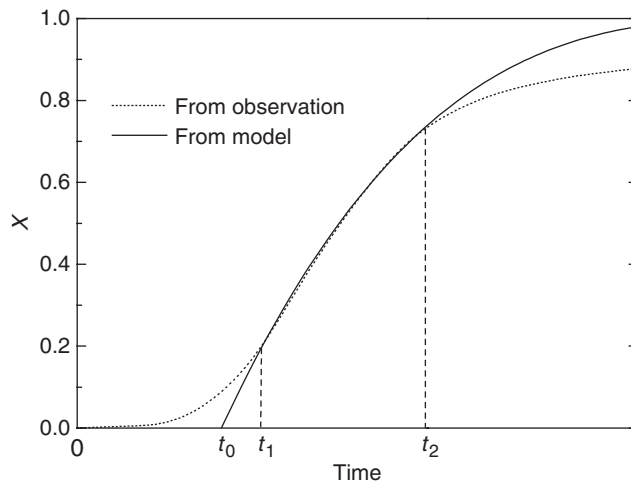


Fig. A1. Time parameter, t_0 , for correction of the induction period.

from t_1 . Let the kinetic model be

$$X = f(t)$$

Then t_0 was the solution for the equation

$$f(t) = 0$$

Acknowledgments

The authors thank H. Katayama and H. Notoya for the BET surface area measurement.

References

- ¹G. A. Slack, R. A. Tanzill, R. O. Pohl, and J. W. Vandersande, "The Intrinsic Thermal Conductivity of AlN," *J. Phys. Chem. Solids*, **48**, 641–7 (1987).
- ²L. M. Sheppard, "Aluminum Nitride: A Versatile But Challenging Material," *Am. Ceram. Soc. Bull.*, **69**, 1801–12 (1990).
- ³A. W. Weimer, *Carbide, Nitride, and Boride Materials Synthesis and Processing*. Chapman & Hall, London, U.K., 1997.
- ⁴A. V. Virkar, T. B. Jackson, and R. A. Cutler, "Thermodynamic and Kinetic Effects of Oxygen Removal on the Thermal Conductivity of Aluminum Nitride," *J. Am. Ceram. Soc.*, **72**, 2031–42 (1989).
- ⁵K. Watari, M. Kawamoto, and K. Ishizaki, "Sintering Chemical Reactions to Increase Thermal Conductivity of Aluminium Nitride," *J. Mater. Sci.*, **26**, 4727–32 (1991).
- ⁶K. Watari, K. Ishizaki, and T. Fujikawa, "Thermal Conduction Mechanism of Aluminium Nitride Ceramics," *J. Mater. Sci.*, **27**, 2627–30 (1992).
- ⁷K. Watari, K. Ishizaki, and F. Tsuchiya, "Phonon Scattering and Thermal Conduction Mechanisms of Sintered Aluminium Nitride Ceramics," *J. Mater. Sci.*, **28**, 3709–14 (1993).
- ⁸J. G. Highfield and P. Bowen, "Diffuse-Reflectance Fourier Transform Infrared Spectroscopic Studies of the Stability of Aluminum Nitride Powder in an Aqueous Environment," *Anal. Chem.*, **61**, 2399–402 (1989).
- ⁹P. Bowen, J. G. Highfield, A. Mocellin, and T. A. Ring, "Degradation of Aluminum Nitride Powder in an Aqueous Environment," *J. Am. Ceram. Soc.*, **73**, 724–8 (1990).
- ¹⁰L. M. Svedberg, K. C. Arndt, and M. J. Cima, "Corrosion of Aluminum Nitride (AlN) in Aqueous Cleaning Solutions," *J. Am. Ceram. Soc.*, **83**, 41–6 (2000).
- ¹¹S. Fukumoto, T. Hookabe, and H. Tsubakino, "Hydrolysis Behavior of Aluminum Nitride in Various Solutions," *J. Mater. Sci.*, **35**, 2743–8 (2000).
- ¹²K. Krnel and T. Kosmac, "Reactivity of Aluminum Nitride Powder in Dilute Inorganic Acids," *J. Am. Ceram. Soc.*, **83**, 1375–8 (2000).
- ¹³Y. Shimizu, S. Takatsuki, and M. Egashira, "Effect of Surface-Oxidation Treatment on the Chemical Stability of Aluminum Nitride Powder," *Nagasaki Daigaku Kogakubu Kenkyu Hokok.*, **19**, 87–93 (1989).
- ¹⁴Y. Li, T. Qiu, and J. Xu, "Effect of Thermal Oxidation Treatment in Air on the Hydrolysis of AlN Powder," *Mater. Res. Bull.*, **32**, 1173–9 (1997).
- ¹⁵Y. Zhang and J. Binner, "Hydrolysis Process of a Surface Treated Aluminum Nitride Powder—A FTIR Study," *J. Mater. Sci. Lett.*, **21**, 803–5 (2002).
- ¹⁶H. B. Shan, Y. Zhu, and Z. T. Zhang, "Surface Treatment and Hydrolysis Kinetics of Organic Films Coated on AlN Powder," *Br. Ceram. Trans.*, **98**, 146–50 (1999).
- ¹⁷F. Barba, P. Ortega, J. Bermudo, M. I. Osendi, and J. S. Moya, "Effect of Oxygen Content on the Corrosion of AlN Powder in Diluted Acid Solution," *J. Eur. Ceram. Soc.*, **13**, 335–8 (1994).
- ¹⁸A. Abid, R. Bensalem, and B. J. Sealy, "The Thermal Stability of Aluminum Nitride," *J. Mater. Sci.*, **21**, 1301–4 (1986).
- ¹⁹Y. Kameshima, S. Kuramochi, A. Yasumori, and K. Okada, "Analysis of Surface State and Stability During Storage of AlN Powders by X-Ray Photoelectron Spectroscopy," *J. Ceram. Soc. Jpn.*, **106**, 749–53 (1998).
- ²⁰N. Saito, Ch. Ishizaki, and K. Ishizaki, "Temperature Programmed Desorption (TPD) Evaluation of Aluminum Nitride Powder Surfaces Produced by Different Manufacturing Processes," *J. Ceram. Soc. Jpn., Int. Ed.*, **102**, 299–302 (1994).
- ²¹N. Saito and K. Ishizaki, "Auger Electron Spectroscopy of Aluminum Nitride Powder Surfaces," *J. Am. Ceram. Soc.*, **79**, 1213–7 (1996).
- ²²J. Li, M. Nakamura, T. Shirai, K. Matsumaru, Ch. Ishizaki, and K. Ishizaki, "Hydrolysis of Aluminum Nitride Powders in Moist Air," *Adv. Tech. Mater. Mater. Proc. J. (ATM)*, **7**, 37–42 (2005).
- ²³R. K. Hart, "The Formation of Films on Aluminium Immersed in Water," *Trans. Faraday Soc.*, **53**, 1020–7 (1957).
- ²⁴T. N. Wittberg, J. D. Wolf, and P. S. Wang, "Aluminum Hydroxide Growth on Aluminum Surfaces Exposed to an Air/1% NO₂ Mixture," *J. Mater. Sci.*, **23**, 1745–7 (1988).
- ²⁵K. Wefers and C. Misra, "Oxides and Hydroxides of Aluminum, Alcoa Technical Paper No. 19, Revised," Alcoa Laboratories, Aluminum Company of America, Pittsburgh, 1987.
- ²⁶Ch. Ishizaki, P. Raharjo, K. Sato, and K. Ishizaki, "Mechanism of Hard Agglomerate Formation in a High Purity Sub-Micron α -Alumina Powder," *J. Ceram. Soc. Jpn.*, **109**, 16–22 (2001).
- ²⁷O. Levenspiel, *Chemical Reaction Engineering*, pp. 357–408. John Wiley & Sons, New York, 1972.
- ²⁸R. E. Carter, "Kinetic Model for Solid-State Reactions," *J. Chem. Phys.*, **34**, 2010–5 (1961).
- ²⁹R. E. Carter, "Kinetic Model for Solid-State Reactions," *J. Chem. Phys.*, **35**, 1137–8 (1961).
- ³⁰W. Jander, "Reactions in Solid State at High Temperatures (in German)," *Z. Anorg. Allg. Chem.*, **163**, 1–30 (1927).
- ³¹S. F. Hulbert, "Models for Solid-State Reactions in Powdered Compacts: A Review," *J. Br. Ceram. Soc.*, **6**, 11–20 (1969). □